LASER INTERFEROMETER GRAVITATIONAL WAVE OBSERVATORY
- LIGO -
CALIFORNIA INSTITUTE OF TECHNOLOGY
MASSACHUSETTS INSTITUTE OF TECHNOLOGY

Document Type	**LIGO-T980029-00 - D**	5/7/98

Effect of Beamsplitter Vibration Resonance Excitation on the Optically Sensed Cavity Length

D. Coyne

Distribution of this draft:

Detector

This is an internal working note
of the LIGO Project.

California Institute of Technology
LIGO Project - MS 51-33
Pasadena CA 91125
Phone (818) 395-2129
Fax (818) 304-9834
E-mail: info@ligo.caltech.edu

Massachusetts Institute of Technology
LIGO Project - MS 20B-145
Cambridge, MA 01239
Phone (617) 253-4824
Fax (617) 253-7014
E-mail: info@ligo.mit.edu

WWW: http://www.ligo.caltech.edu/

Abstract

Any (unintended) magnetic coil drive currents at the beamsplitter resonances will be amplified by the high Q of the beamsplitter. The transfer function of applied force at the magnet positions to TEM_{00} displacement response of the front surface of the LIGO beamsplitter is calculated (based upon finite element structural dynamics computation). The gain attentuation required in the length control system, in order to prevent driving the beamsplitter motion at resonance beyond acceptable limits, may be established from the transfer function.

Keywords: beamsplitter, eigenvectors, mode shapes, frequencies, length control, LSC

1 INTRODUCTION

The analytical derivation of the effect upon the TEM_{00} cavity mode due to driving the beamsplitter at one or more of it's resonance frequencies has been described in a previous technical memorandum[1] on the End Test Mass (ETM). This same methodology is applied here to the beamsplitter (BS) which has lower resonant frequencies.

2 BEAMSPLITTER FINITE ELEMENT MODEL

The Beamsplitter (BS) finite element model is indicated in Figure 1. The optic is a 250 mm diameter, 40 mm thick (at it's minimum) fused silica cylinder with one face wedged at a 1 degree angle[2]. The 50/50 beam splitting coating is on the front face and the magnet/standoff assemblies (used for voice coil actuation and control) are on the back face. The model is composed of 6240 linear solid brick elements and has the mass properties shown in Figure 1.

Figure (1) Finite Element Model, Coordinate System and Mass Properties (units are mm and kg)

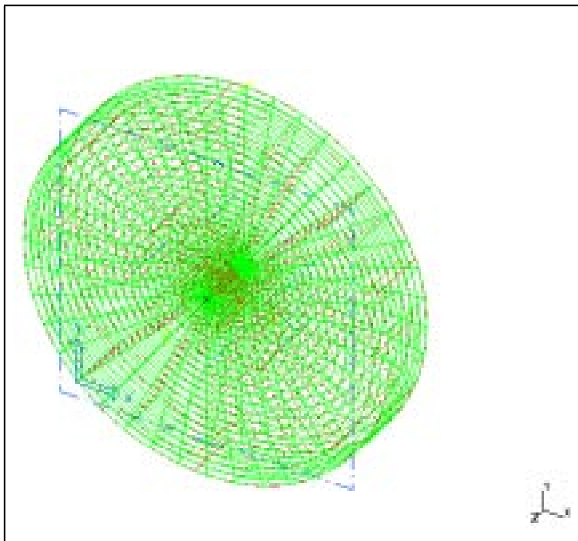

```
Volume            :  2.062D+06
Mass              :  4.541D+00
Center of gravity : -8.911D-06   1.605D+00  -2.110D+01
Moments of Inertia about c.g.
  Ixx  Iyy  Izz   :  1.825D+04   1.827D+04   3.520D+04
  Ixy  Iyz  Izx   :  1.965D-03  -1.536D+02   6.254D-05
Moments of Inertia about origin
  Ixx  Iyy  Izz   :  2.029D+04   2.029D+04   3.522D+04
  Ixy  Iyz  Izx   :  1.901D-03  -3.074D+02   9.165D-04
Principal axes
  1 :  1.000  0.000  0.000
  2 :  0.000 -1.000  0.009
  3 :  0.000  0.009  1.000
Principal Moments of Inertia
  I11  I22  I33   :  1.825D+04   1.826D+04   3.521D+04
```

The four magnet positions are at a radial distance of 114.3 mm and at 45, 135, 225 and 315 degrees from the +X (horizontal) axis. The dynamic model does not include the beveled edge of

1. D. Coyne, “Test Mass Transmissibility”, LIGO-T970191-03, 2/10/98.
2. LIGO Drawing D960789-B, Beam Splitter Substrate.

the optic, nor does it include the four dumbbell magnet standoff and magnet assemblies. The boundary condition for the eigenvalue analysis is free (unconstrained); The first six modes are zero frequency, rigid body modes.

The material property data used for the fused silica is indicated in Table 2.

Table 1. Fused Silica Property Data

Property	*Units*	*Value*
Elastic Extensional Modulus, E	mN/mm^2	7.3×10^7
Elastic Shear Modulus, $G = \frac{E}{2(1+\nu)}$	mN/mm^2	3.1×10^7
Poison's ratio, ν	-	0.17
Density, ρ	Kg/mm^3	2.202×10^{-6}
Quality factor[a], Q	-	1.3×10^6

a. S. Kawamura, et. al., LIGO-T970158-06-D

3 NATURAL MODES

The natural modes shapes, frequencies, modal mass and modal stiffness are indicated in Table 1. The analysis indicates a non-axisymmetric pair of modes with astigmatic shape at 3.78 kHz, the first symmetric (drum head) mode at 5.58 kHz, then 5 pairs of non-axisymmetric modes before the second symmetric (radial contraction) mode at 14.6 kHz. By comparison, the ETM has two astigmatic modes at 6.6 kHz, a drum head mode at 9.2 kHz, then 4 pairs of non-axisymmetric modes before the radial contraction mode at 14.5 kHz. Since the BS is thinner then the ETM, it's bending stiffness is reduced and the lower BS frequency of the drum head mode and the additional non-axisymmetric mode pair between the 1st and 2nd symmetric modes is expected.

The eigenvalue analysis results presented herein are the result of a "consistent" mass matrix formulation, rather than a "lumped" mass matrix.[1] Previous analysis (Ref. [1]), on the Input Test Mass (ITM) was based upon a lumped mass matrix. For the BS, the frequencies calculated with a consistent mass matrix (i.e. the more realistic case) are from 1% to 6% higher than the lumped mass case; This may explain the ~1% lower first frequency by analysis compared to measurement reported in Ref. [1] for the ETM.

1. See for example, K. Bathe, Finite Element Procedures in Engineering Analysis, Prentice-Hall, 1982, pp. 162-163, for an explanation of consistent and lumped mass matrices.

Table 2. BS Calculated Modes

#	*Mode Shape*	*Frequency (Hz)*	*Modal Mass (10^6 gm)*	*Modal Stiffness (10^{15} N/m)*
7	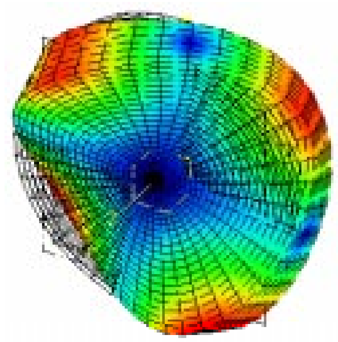	3785	0.865	0.489
8	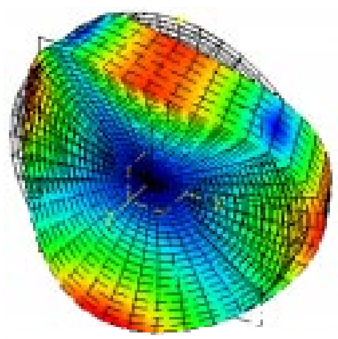	3785	0.851	0.481
9	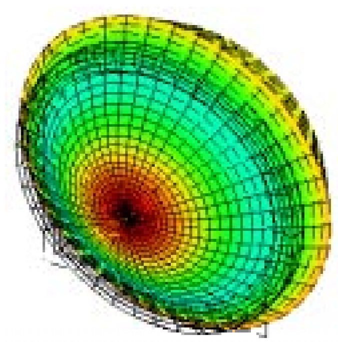	5578	1.25	1.54

Table 2. BS Calculated Modes

#	Mode Shape	*Frequency (Hz)*	*Modal Mass (10^6 gm)*	*Modal Stiffness (10^{15} N/m)*
10	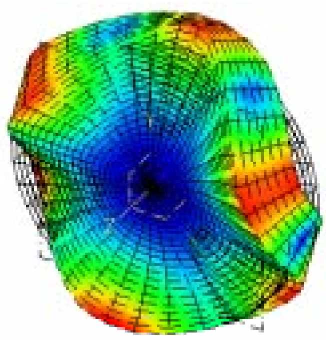	7975	0.735	1.85
11	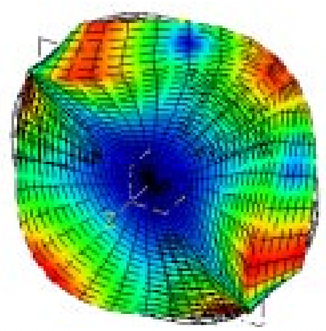	7975	0.756	1.90
12	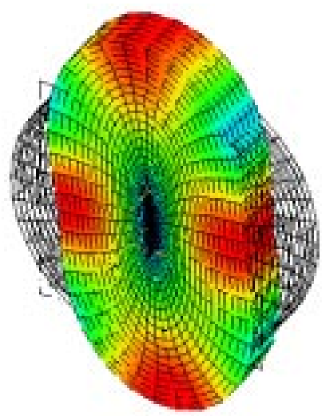	11259	2.17	10.9

Table 2. BS Calculated Modes

#	*Mode Shape*	*Frequency (Hz)*	*Modal Mass* (10^6 *gm)*	*Modal Stiffness* (10^{15} *N/m)*
13	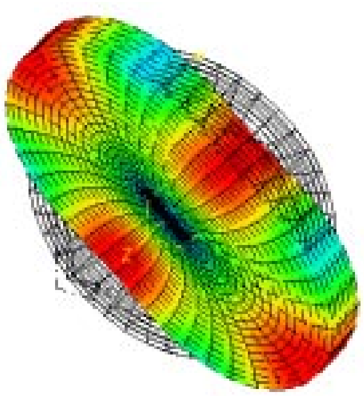	11259	3.26	16.3
14	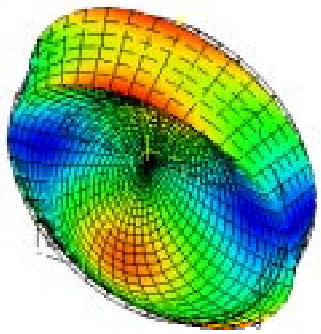	11332	1.08	5.47
15	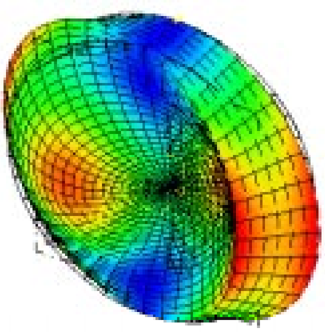	11334	1.13	5.73

Table 2. BS Calculated Modes

#	*Mode Shape*	*Frequency (Hz)*	*Modal Mass* (10^6 *gm)*	*Modal Stiffness* (10^{15} *N/m)*
16	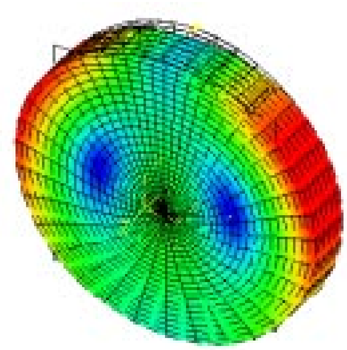	12674	1.16	7.34
17	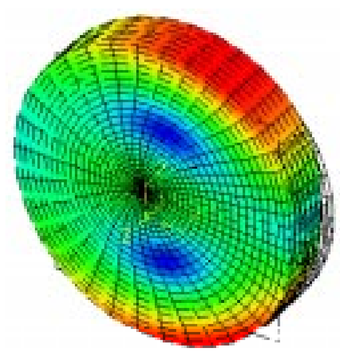	12677	1.11	7.07
18	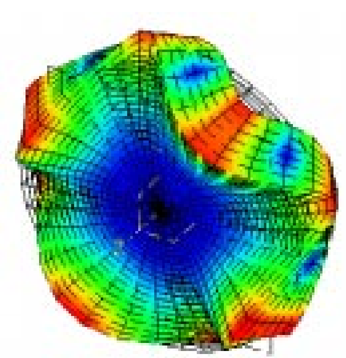	12760	0.702	4.51

Table 2. BS Calculated Modes

#	*Mode Shape*	*Frequency (Hz)*	*Modal Mass (10^6 gm)*	*Modal Stiffness (10^{15} N/m)*
19	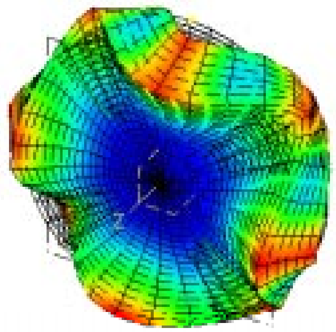	12760	0.651	4.18
20	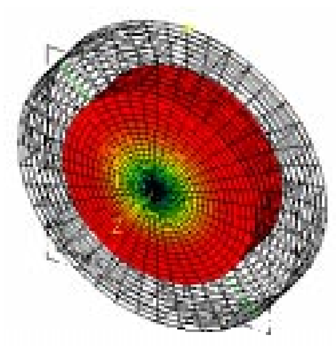	14629	3.20	27.1
21	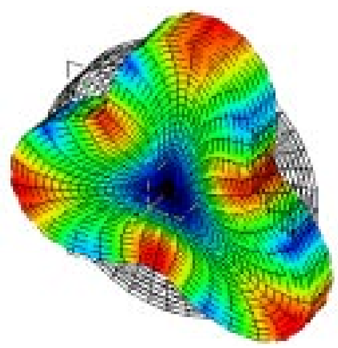	17283	1.46	17.2
22	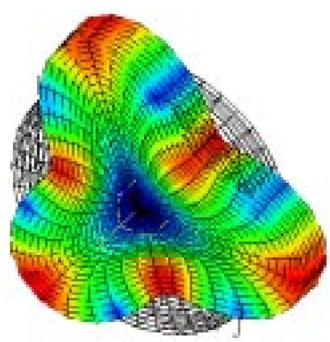	17283	1.56	18.3

Table 2. BS Calculated Modes

#	*Mode Shape*	*Frequency (Hz)*	*Modal Mass (10^6 gm)*	*Modal Stiffness (10^{15} N/m)*
23	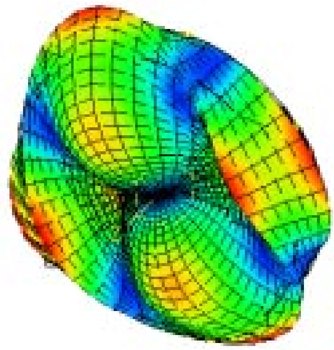	17388	1.15	13.7
24	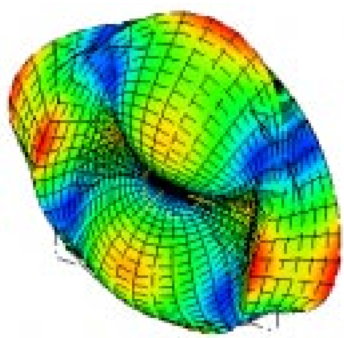	17388	1.15	13.8
25	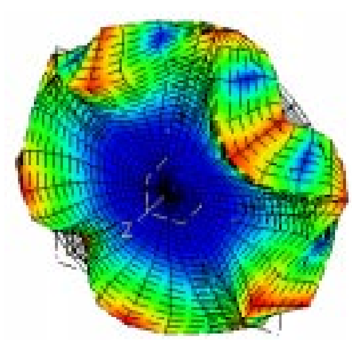	17958	0.575	7.32
26	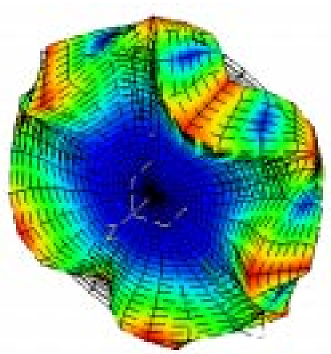	17958	0.576	7.33

4 TRANSFER FUNCTION

In the frequency response analysis, the magnet/voice coil force is assumed to act in the direction parallel to the beamsplitter cylindrical axis despite the fact that the magnet's axis is normal to the wedged surface. The steady-state transfer function (ratio of response displacement to driving force) is given for coherently forcing at the four magnet positions (on the backface of the beamsplitter) with response at the 21 points (on the front face of the beamsplitter) indicated in Figure 2.

Figure (2) Response & Excitation Points

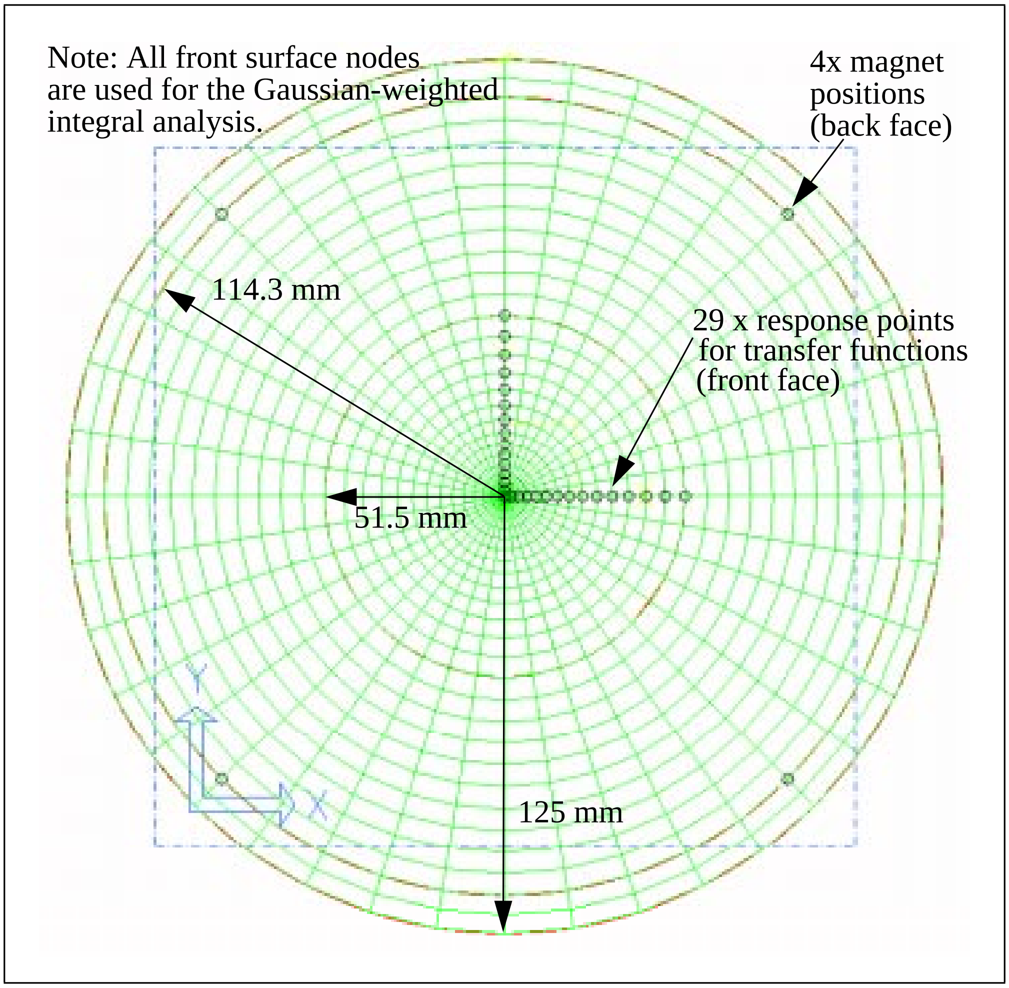

The resulting transfer functions (surface point displacements for magnet point forces) are indicated in Figure 3, as calculated by the IDEAS dynamic response module. The amplitude of response at resonance is not calculated well in these transfer functions for high-Q systems such as the beamsplitter. The frequency sampling, $\Delta\omega$, required to capture the amplitude at resonance, ω_0, is approximately:

$$\frac{\Delta\omega}{\omega_0} \approx \frac{1}{Q} \qquad (1)$$

For a Q=1 x 10^6, and a resonance of f_0 = 5 kHz, this implies Δf ~ 5 mHz or 3 million samples over a 15 kHz range, which is a prohibitively long calculation.

The frequency response can be computed through the summation of modal responses:

$$\{\gamma\} = \sum_{k=1}^{n} \frac{\{F_k\}}{m_k(\omega_k^2 + 2i\zeta\omega\omega_k - \omega^2)} \tag{2}$$

where,

m_k = modal mass
γ = modal displacement
ζ = effective modal viscous damping ratio
ω_k = natural frequency
F_k = modal (generalized) force
ω = frequency
subscript k = k^{th} *mode*

At a resonance frequency, ω_0:

$$\{\gamma(\omega_0)\} = \sum_{k=1}^{n} \frac{\{F_k\}}{m_k(\omega_k^2 + 2i\zeta\omega_0\omega_k - \omega_0^2)} \tag{3}$$

or, approximately,

$$\gamma_0 = \frac{F_0}{2im_0\omega_0^2\zeta} \tag{4}$$

The generalized forces (for unrestrained boundary conditions) are:

$$\{F_k\} = [\varphi]^T\{F_e\} \tag{5}$$

where,

$[\varphi]^T$ = mode displacement matrix (mode shapes)
$\{F_e\}$ = applied forces (excitation)

Similarly, the physical displacement is given by:

$$\{\delta\} = [\varphi]^T\{\gamma\} \tag{6}$$

or, the displacement at a response point, r, at resonance, ω_0, is given as follows:

$$\delta_{r0} = \varphi_{r0}\gamma_0 = \varphi_{r0}\left(\frac{F_0}{2im_0\zeta\omega_0^2}\right) = \varphi_{r0}\left(\frac{\{\varphi_0\}^T\{F_e\}}{2im_0\zeta\omega_0^2}\right) \quad (7)$$

$$|\delta_{r0}| = \varphi_{r0}\left(\frac{\{\varphi_0\}^T\{F_e\}}{2m_0\zeta\omega_0^2}\right) \quad (8)$$

If we denote the modal coefficients at each of the 4 magnet positions at the resonance, ω_k, as $\{\varphi_{ke1},\varphi_{ke2},\varphi_{ke3},\varphi_{ke4}\}$ then the transfer function at a response position, δ_r, for a unit force (at each of the 4 magnet positions) is as follows:

$$T_{\delta_r k} = \frac{\varphi_{rk}(\varphi_{ke_1} + \varphi_{ke_2} + \varphi_{ke_3} + \varphi_{ke_4})}{2m_k\zeta\omega_k^2} \quad (9)$$

where:

$$\zeta = \frac{1}{2Q} = 3.8\times10^{-7} \quad (10)$$

Numerical values for $\{\varphi_{ke1},\varphi_{ke2},\varphi_{ke3},\varphi_{ke4}\}$, m_k, φ_{kr} and $T_{\delta_r k}$ for each resonance is given in Table 3 for r = the center of the front face of the beamsplitter.

.

Figure (3) Magnet z-force to surface z-Displacement Transfer Function

15 points along the +x-axis (uneven sampling from the center to a radius of 52 mm)

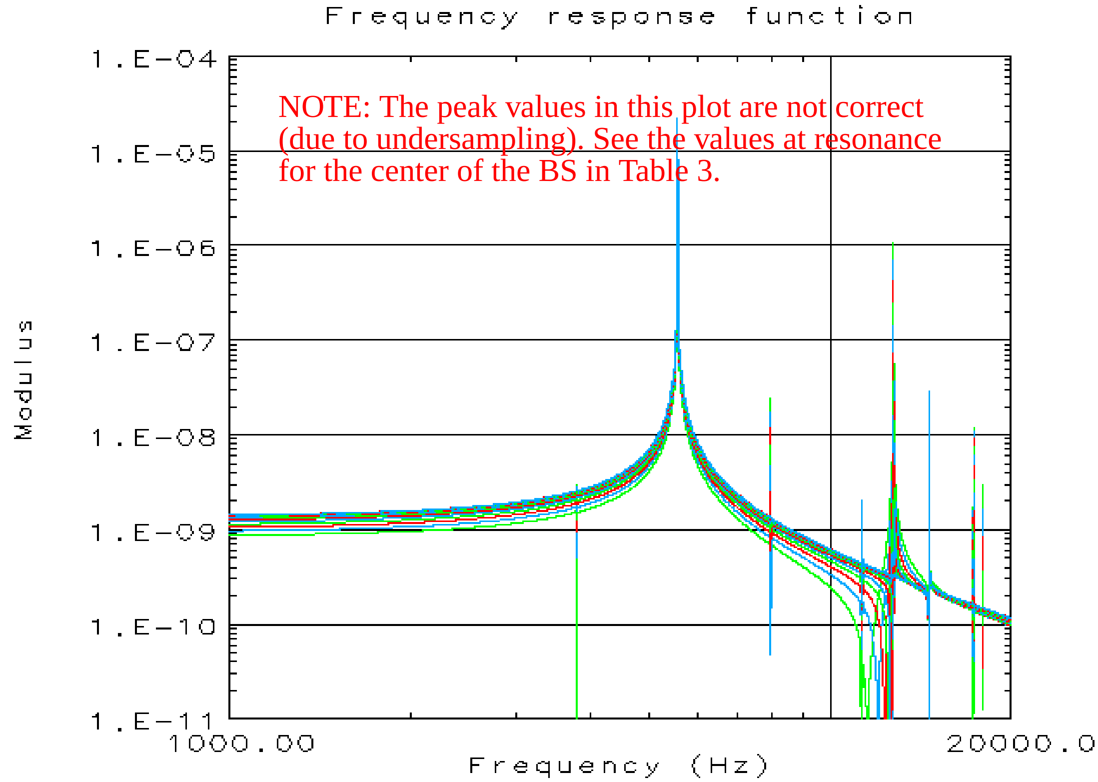

15 points along the +y-axis (uneven sampling from the center to a radius of 52 mm)

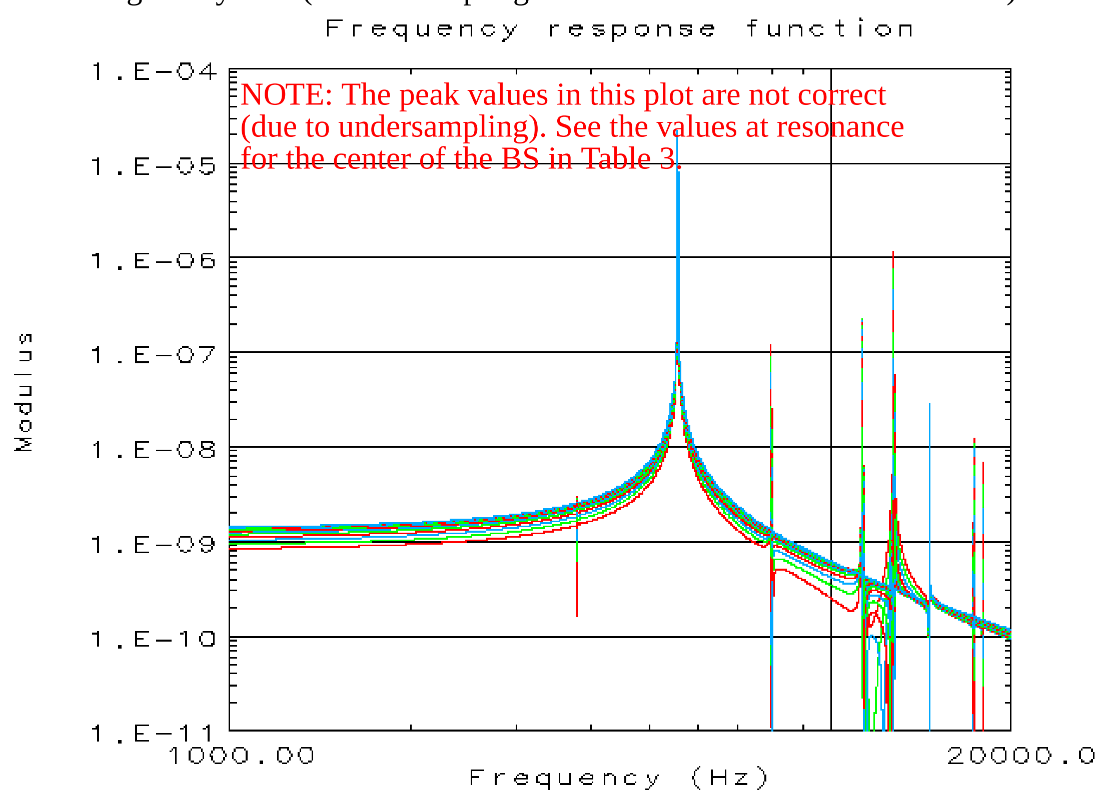

5 MODE INTEGRAL OVERLAP WITH A GAUSSIAN

The derivation of the mode integral overlap with the TEM_{00} beam has been derived previously in Ref. [1] for a normally incident beam; Here the derivation is extended to the non-normal incidence case of the beamsplitter. The cavity length change due to beamsplitter modal motion is sensed by a phase shift imparted to the TEM_{00} mode, described by the Hermite-Gaussian function ψ_{00}. The sensed length change is given by[1]:

$$\delta_{\vec{r}k} = |\vec{k}| \int_S \psi^*_{00}\psi_{00} \frac{(\vec{u} \bullet \hat{n})}{(\vec{k} \bullet \hat{n})} dS \qquad (11)$$

where $\vec{k}$ is the wave vector, $\hat{n}$ is the nominal surface normal unit vector, and $\vec{u}$ is the surface deformation vector. The product,

$$\psi^*_{00}\psi_{00} = I(\vec{r}) \qquad (12)$$

where the Gaussian intensity distribution (normalized over the integral) is:

$$I(\vec{r}) = \left(\frac{2}{\pi w^2}\right) e^{-2\left(\frac{s}{w}\right)^2} = \left(\frac{2}{\pi w^2}\right) e^{\frac{-2[2x^2 + y^2]}{w^2}} \qquad (13)$$

where the beam waist, w = 36.4 mm in the recycling cavity[2]. In this expression, s is the radial (transverse) coordinate to the wave vector. When performing the integral over the optic surface, S, the radial coordinate must be transformed into the x and y coordinates on the face of the beamsplitter, which is nominally at a 45 degree incidence angle (hence the second equality above, where the reflection is taken about the y-axis).

The physical displacement at a position, r, on the BS surface is related to the modal displacement as follows (from Equation 5):

$$\delta_{\vec{r}k} = \varphi_{\vec{r}k}\gamma_k = \varphi_{\vec{r}k}(T_{\gamma_k}F_e) = T_{\delta_{\vec{r}}k}F_e \qquad (14)$$

where the transfer function from coherent force excitation at the four magnet positions to the kth

1. The expression for the length change given in A. Gillespie and F. Raab, "Thermally excited vibrations of the mirrors of laser interferometer gravitational-wave detectors", Phys. Rev. D 52, 577(1995),

$$\text{length change} = |\vec{k}|^{-1} \int_S \psi^*_{00}\psi_{00}(\vec{k} \bullet \vec{u}) dS$$

is not correct in the general case of non-normal incidence. Displacement of the surface in the plane of the surface does not result in a cavity length reduction.

2. W. Kells, Core Optics Design Requirements, LIGO-T950099-04.

modal amplitude is:

$$T_{\gamma_k} = \frac{(\varphi_{ke_1} + \varphi_{ke_2} + \varphi_{ke_3} + \varphi_{ke_4})}{2m_k\zeta_k\omega_k^2} \tag{15}$$

and the transfer function from coherent force excitation at the four magnet positions to displacement at position r due to the kth mode is:

$$T_{\delta_{\vec{r}}k} = \varphi_{\vec{r}k}T_{\gamma_k} \tag{16}$$

The intensity weighted integral of motion due to the kth mode, over surface S, is given by:

$$\Delta_k = \int_S \delta_{\vec{r}k} I(\vec{r} - \vec{r}_o)dA = T_{\gamma_k}F_e\int_S \varphi_{\vec{r}k} I(\vec{r} - \vec{r}_o)dA \tag{17}$$

where the intensity distribution may be decentered by an alignment tolerance of r_o = 1 mm:

$$\vec{r}_o = (r_o\cos\theta)\hat{i} + (r_o\sin\theta)\hat{j} \tag{18}$$

where i and j are unit vectors in the x and y coordinate directions.

The kth mode integral overlap transfer function is then:

$$T_{\Delta_k} = \frac{\Delta_k}{F_e} = T_{\gamma_k}\int_S \varphi_{\vec{r}k} I(\vec{r} - \vec{r}_o)dA = T_{\gamma_k}\Gamma_k(\theta) \tag{19}$$

The maximum value of the transfer function over all values of θ is defined as:

$$max_\theta[T_{\Delta_k}] = T_{\gamma_k} max_\theta[\Gamma_k(\theta)] \tag{20}$$

The integrals were performed in Matlab. The IDEAS finite element model (nodal positions, surface node numbers) and mode shapes were imported into Matlab. A two-dimensional spline fit to the non-uniform finite element nodal grid was used to calculate the mode shape on a finer grid within central region of ± 2.4 beam waists (i.e. the surface S). The results (and the input and some of the intermediate values in the calculation) are given in Tables 3 and 4. The interpolated central regions, S, of the mode shapes are displayed in Table 5.

The Gaussian weighted integral transfer functions for the first 20 elastic modes are given in Table 4 for two conditions. The first condition is for a laser beam centered on the front face of the beamsplitter but with a radial alignment uncertainty of 1 mm. The second condition is an intentional horizontal (x-axis) offset (of 12 mm) such that with refraction through the beamsplitter the chief ray goes through the center of the beamsplitter, as well as a radial alignment uncertainty of 1 mm.

The transfer function at the BS first symmetric mode (5578 Hz) is about 10 times greater than for the ITM at its first symmetric mode (9205 Hz). The effect of the BS higher response, relative to the ETM, is mitigated by the finesse of the Fabry-Perot arm cavity.

Table 3. Front Surface Center Transfer Function (modal damping, $\zeta = 3.8 \times 10^{-7}$)

k	*Frequency (Hz)*	*Modal Mass (10^6 gm)*	*Mode Shape Amplitude at Magnet Positions*				*Modal Transfer Function* T_{γ_k}	*Mode Shape Amplitude at the Center* φ_{kr}	*Center Displacement* $T_{\delta_r k}$ *(m/N)*
			φ_{ke_1}	φ_{ke_2}	φ_{ke_3}	φ_{ke_4}			
7	3784.9	8.65e+05	-770.53	769.90	817.05	-816.13	7.72e-10	-332.51	-2.57e-07
8	3784.9	8.51e+05	260.66	-262.49	-276.00	278.65	2.23e-09	243.77	5.44e-07
9	5578.2	1.25e+06	-527.56	-527.56	-562.12	-562.12	-1.87e-06	151.04	-2.82e-04
10	7974.7	7.35e+05	246.17	729.02	-778.86	-286.95	-6.46e-08	-44.07	2.85e-06
11	7974.8	7.56e+05	-748.33	275.57	-263.23	779.93	3.05e-08	-313.70	-9.56e-06
12	11259.1	2.17e+06	10.34	18.61	-15.25	-15.16	-1.77e-10	-21.41	3.78e-09
13	11259.1	3.26e+06	-27.35	19.70	3.75	4.28	3.09e-11	35.19	1.09e-09
14	11332.3	1.08e+06	371.77	371.60	-387.98	-388.18	-7.88e-09	-492.48	3.88e-06
15	11334.2	1.13e+06	371.40	-371.59	405.78	-405.58	2.07e-12	-363.88	-7.52e-10
16	12674.4	1.16e+06	-29.80	-29.81	23.89	23.87	-2.12e-09	17.73	-3.75e-08
17	12677.4	1.11e+06	-21.77	21.69	-31.35	31.30	-2.24e-11	14.51	-3.25e-10
18	12760.0	7.02e+05	457.64	418.74	481.24	439.72	5.24e-07	235.12	1.23e-04
19	12760.1	6.51e+05	-611.23	-636.55	-642.13	-669.20	-8.05e-07	-76.96	6.19e-05
20	14628.5	3.20e+06	-35.04	-35.04	-46.48	-46.48	-7.93e-09	59.76	-4.74e-07
21	17283.2	1.46e+06	3.93	-31.62	21.75	21.08	1.16e-09	-33.87	-3.92e-08
22	17283.3	1.56e+06	-41.21	25.42	11.60	12.82	6.17e-10	39.63	2.45e-08
23	17388.4	1.15e+06	385.10	-394.31	-412.13	421.19	-1.36e-11	-580.75	7.90e-09

Table 3. Front Surface Center Transfer Function (modal damping, $\zeta = 3.8 \times 10^{-7}$)

k	*Frequency (Hz)*	*Modal Mass (10^6 gm)*	*Mode Shape Amplitude at Magnet Positions*				*Modal Transfer Function* T_{γ_k}	*Mode Shape Amplitude at the Center* φ_{kr}	*Center Displacement* $T_{\delta_r k}$ *(m/N)*
			φ_{ke_1}	φ_{ke_2}	φ_{ke_3}	φ_{ke_4}			
24	17388.4	1.15e+06	-212.33	194.82	226.25	-209.07	-3.09e-11	606.65	-1.87e-08
25	17958.0	5.75e+05	728.49	3.59	55.42	-764.36	4.16e-09	120.00	4.99e-07
26	17958.3	5.76e+05	52.53	730.77	-762.80	4.32	4.45e-09	135.46	6.03e-07

Table 4. Gaussian Weighted Integral Transfer Function

k	*Frequency (Hz)*	*Value of the Integral with no Gaussian Intensity Distribution offset* $\Gamma_k(r_o \to 0)$	*Centered* ⌖ | ⌀ *1 mm*		*Refractive Offset (12 mm offset in x* ⌖ | ⌀ *1 mm*	
			Maximum Value of the Integral vs. θ $max_\theta[\Gamma_k(\theta)]$	*Gaussian Weighted Integral Transfer Function* $max_\theta[T_{\Delta_k}]$ *(m/N)*	*Maximum Value of the Integral vs.* θ $max_\theta[\Gamma_k(\theta)]$	*Gaussian Weighted Integral Transfer Function* $max_\theta[T_{\Delta_k}]$ *(m/N)*
7	3784.9	4.131	4.336	3.35e-09	3.920	3.03e-09
8	3784.9	12.007	12.224	2.73e-08	2.575	5.75e-09
9	5578.2	893.064	893.143	-1.67e-03	873.596	-1.63e-03
10	7974.7	0.052	0.449	-2.90e-08	1.471	-9.51e-08
11	7974.8	-0.021	0.425	1.29e-08	3.140	9.56e-08
12	11259.1	-0.174	1.303	-2.30e-10	3.948	-6.97e-10
13	11259.1	0.046	1.467	4.52e-11	17.916	5.53e-10
14	11332.3	-1.554	26.134	-2.06e-07	25.681	-2.02e-07
15	11334.2	-0.006	26.652	5.51e-11	336.297	6.95e-10
16	12674.4	3.312	3.749	-7.94e-09	3.564	-7.55e-09
17	12677.4	0.001	0.431	-9.63e-12	5.571	-1.25e-10
18	12760.0	-0.384	0.394	2.06e-07	0.362	1.90e-07
19	12760.1	0.558	0.566	-4.56e-07	0.403	-3.24e-07
20	14628.5	114.422	114.492	-9.08e-07	113.565	-9.01e-07
21	17283.2	-2.963	2.999	3.47e-09	0.750	8.69e-10
22	17283.3	-1.691	1.728	1.07e-09	0.604	3.73e-10

Table 4. Gaussian Weighted Integral Transfer Function

k	*Frequency (Hz)*	*Value of the Integral with no Gaussian Intensity Distribution offset* $\Gamma_k(r_o \to 0)$	*Centered* ⌖ ∅1 mm		*Refractive Offset (12 mm offset in x* ⌖ ∅1 mm	
			Maximum Value of the Integral vs. θ $max_\theta[\Gamma_k(\theta)]$	*Gaussian Weighted Integral Transfer Function* $max_\theta[T_{\Delta_k}]$ *(m/N)*	*Maximum Value of the Integral vs.* θ $max_\theta[\Gamma_k(\theta)]$	*Gaussian Weighted Integral Transfer Function* $max_\theta[T_{\Delta_k}]$ *(m/N)*
23	17388.4	31.026	31.568	-4.30e-10	10.612	-1.44e-10
24	17388.4	59.528	60.067	-1.85e-09	14.029	-4.33e-10
25	17958.0	0.006	0.039	1.64e-10	0.126	5.23e-10
26	17958.3	0.004	0.037	1.65e-10	0.153	6.81e-10

The table below shows the interpolated surface displacements for each of the first 20 elastic modes of the beamsplitter.

Table 5. Interpolated Mode Shapes for Z-displacement of the Front Surface Central Region (± 2.43 w)

k	*Frequency (Hz)*	*Surface Plot*	*Contour Plot*
7	3785	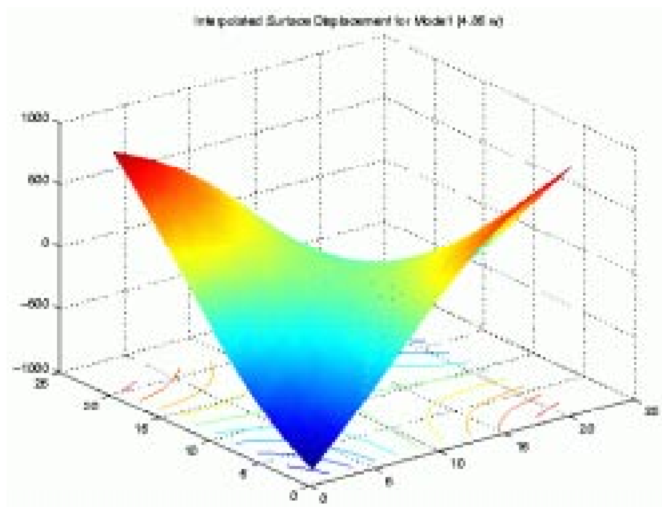	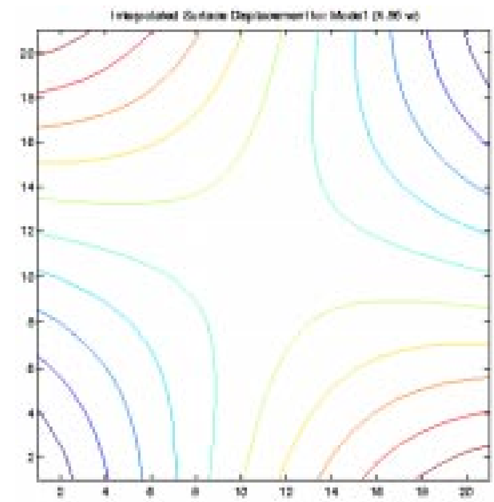
8	3785	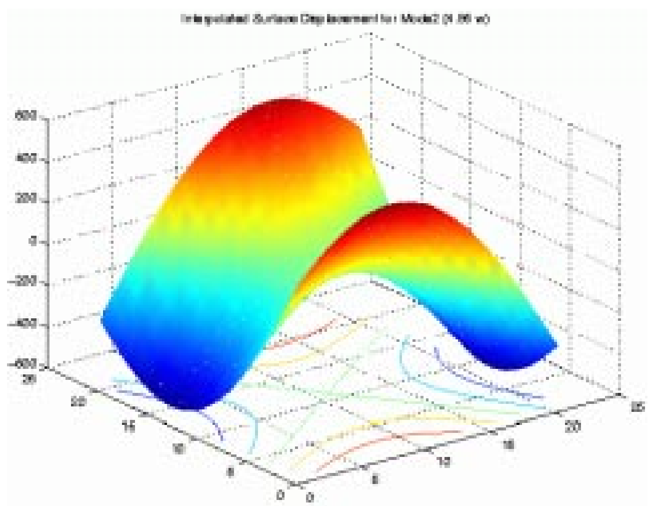	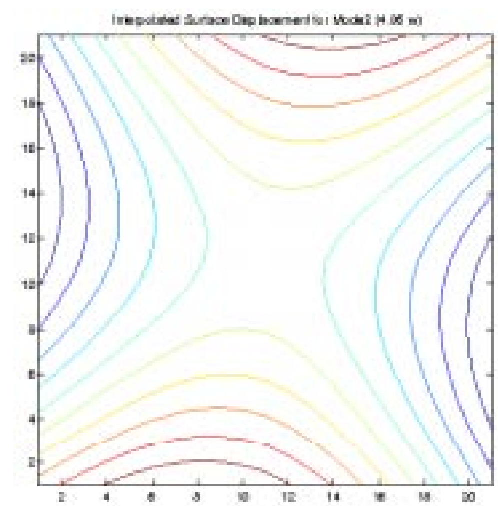

Table 5. Interpolated Mode Shapes for Z-displacement of the Front Surface Central Region (± 2.43 w)

k	*Frequency (Hz)*	*Surface Plot*	*Contour Plot*
9	5578	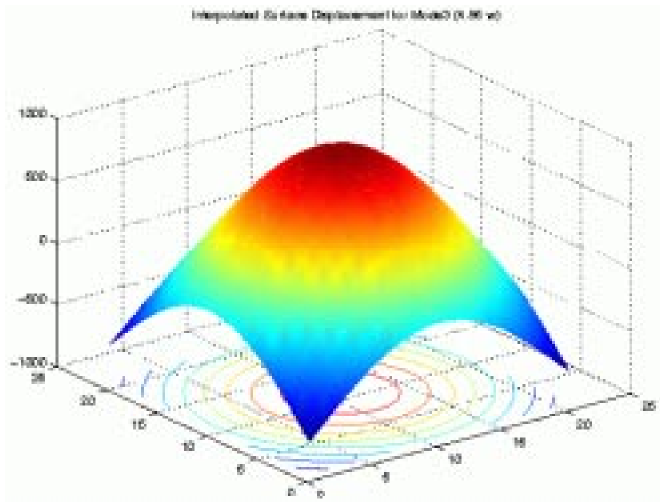	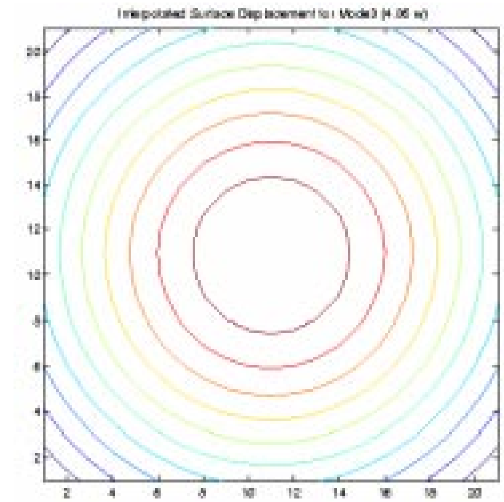

Table 5. Interpolated Mode Shapes for Z-displacement of the Front Surface Central Region (± 2.43 w)

k	*Frequency (Hz)*	*Surface Plot*	*Contour Plot*
10	7975	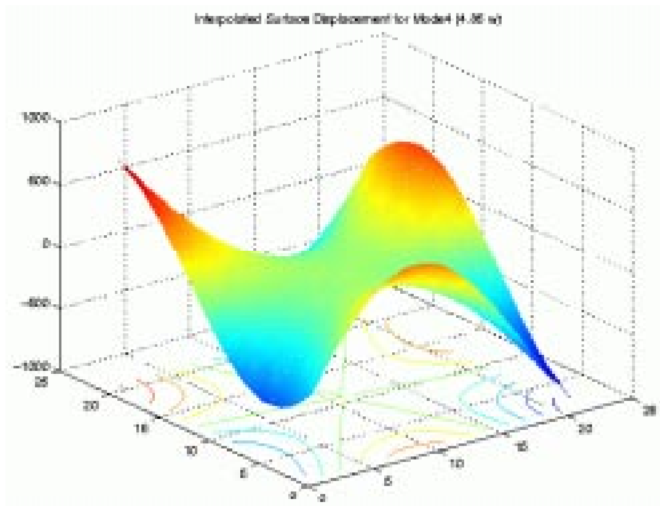	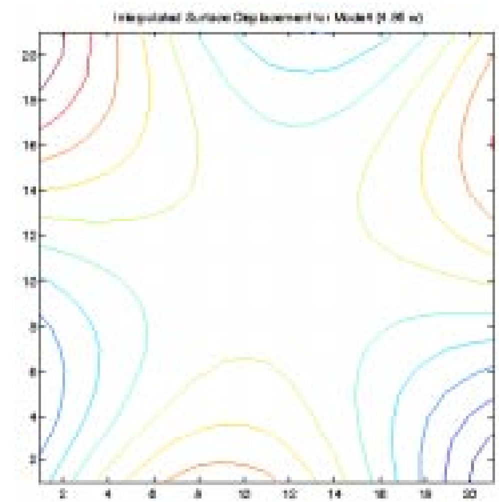
11	7975	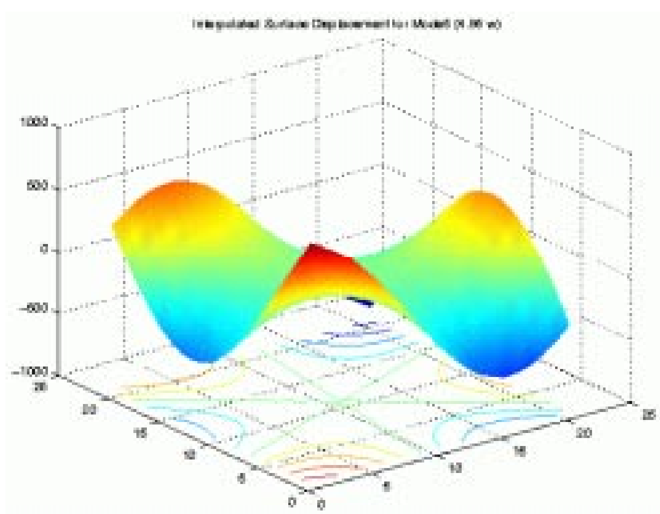	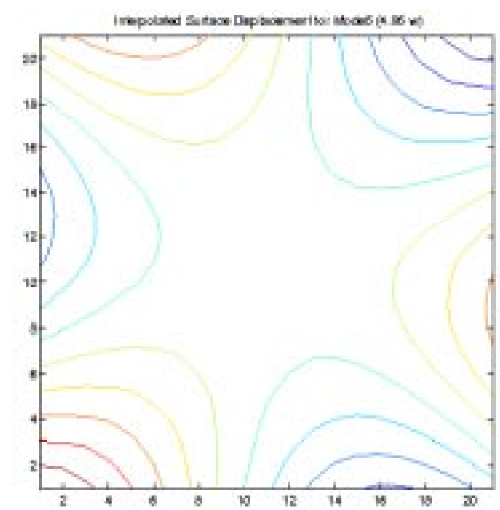

Table 5. Interpolated Mode Shapes for Z-displacement of the Front Surface Central Region (± 2.43 w)

k	*Frequency (Hz)*	*Surface Plot*	*Contour Plot*
12	11259	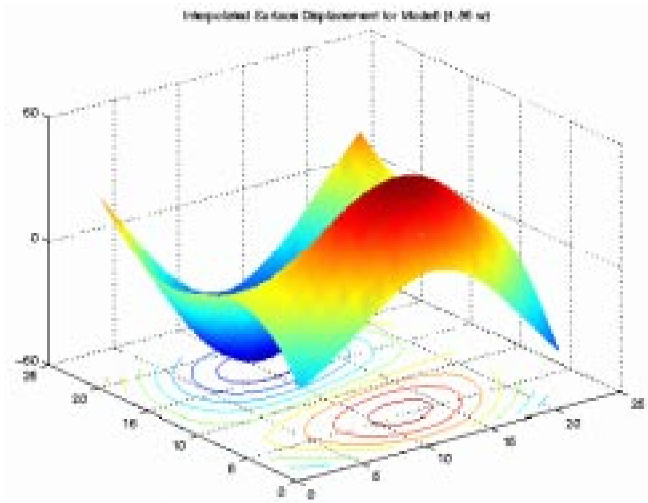	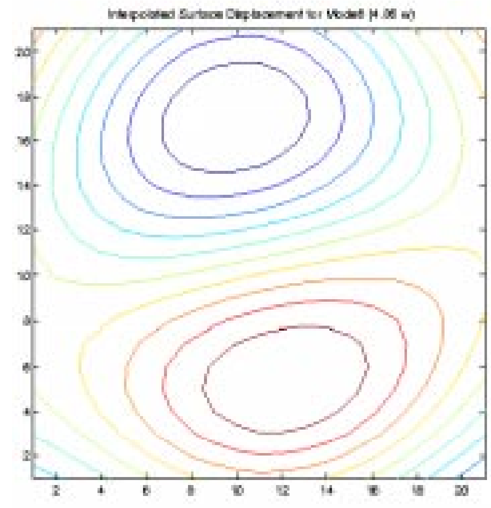
13	11259	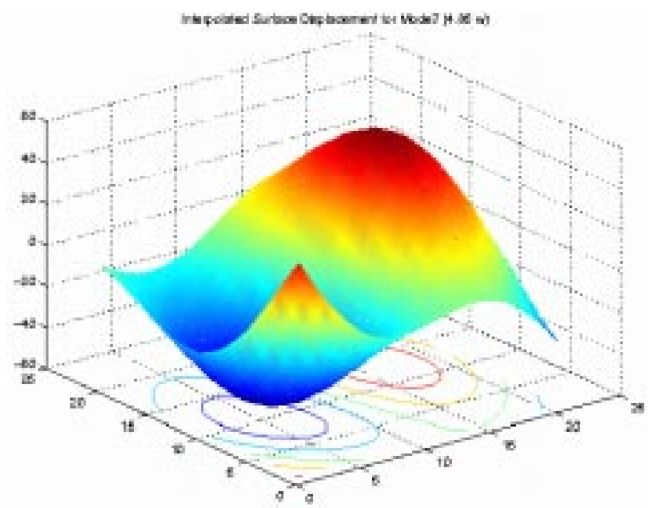	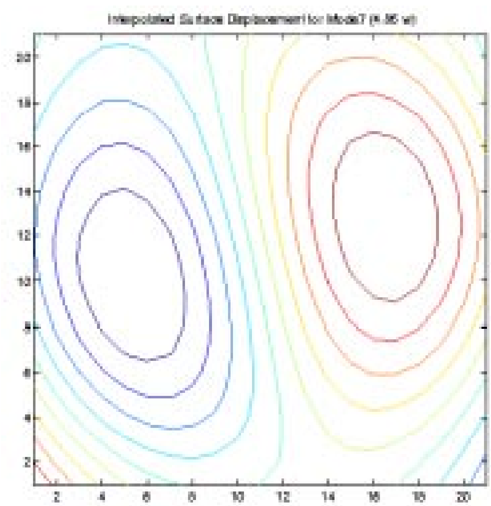

Table 5. Interpolated Mode Shapes for Z-displacement of the Front Surface Central Region (± 2.43 w)

k	*Frequency (Hz)*	*Surface Plot*	*Contour Plot*
14	11332	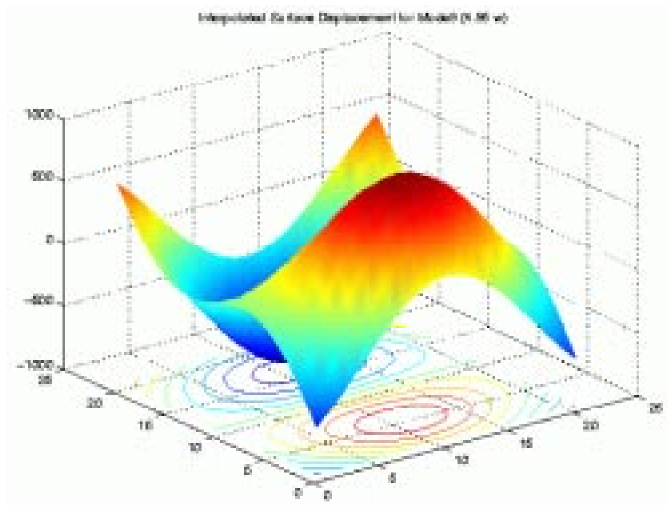	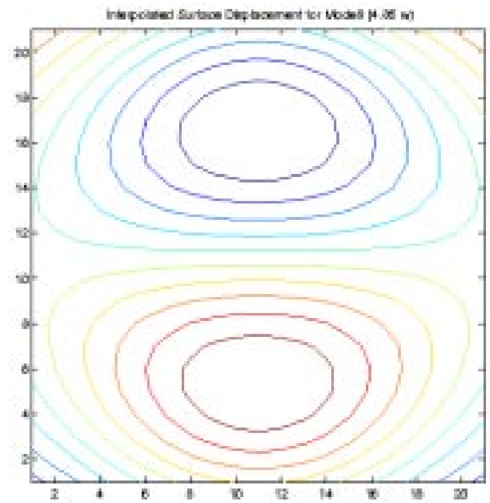
15	11334	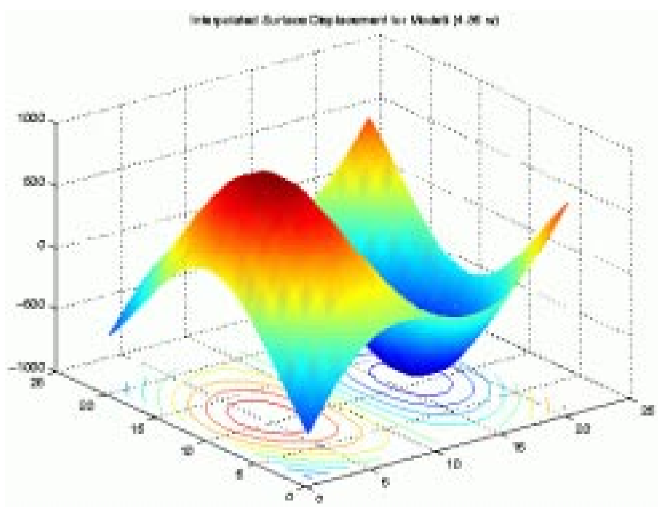	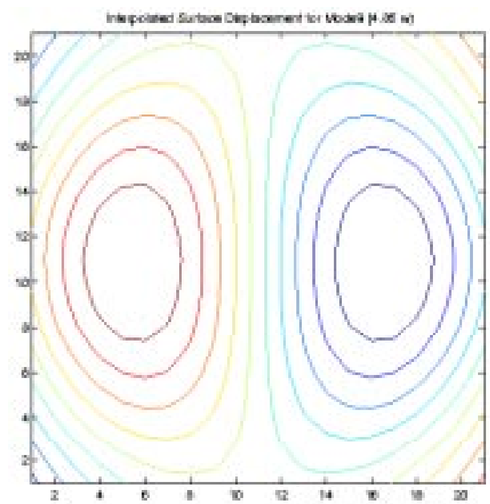

Table 5. Interpolated Mode Shapes for Z-displacement of the Front Surface Central Region (± 2.43 w)

k	*Frequency (Hz)*	*Surface Plot*	*Contour Plot*
16	12674	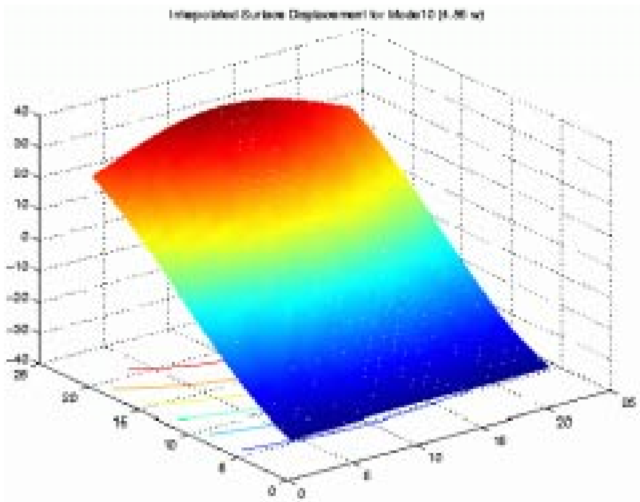	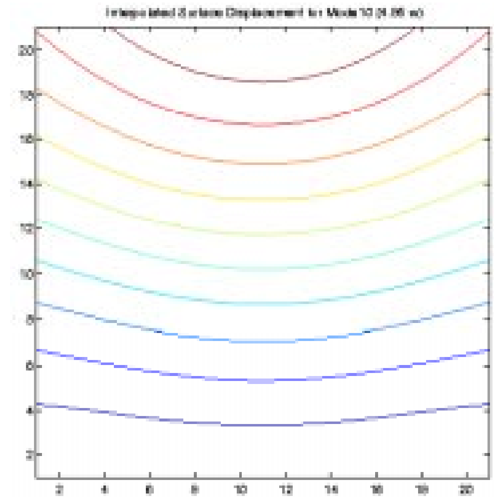
17	12677	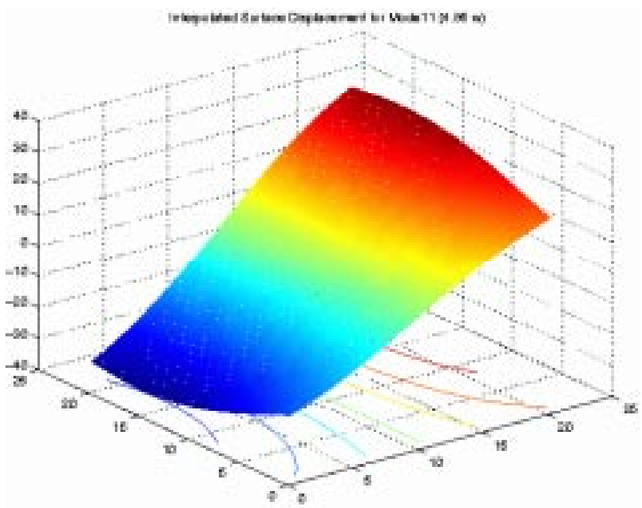	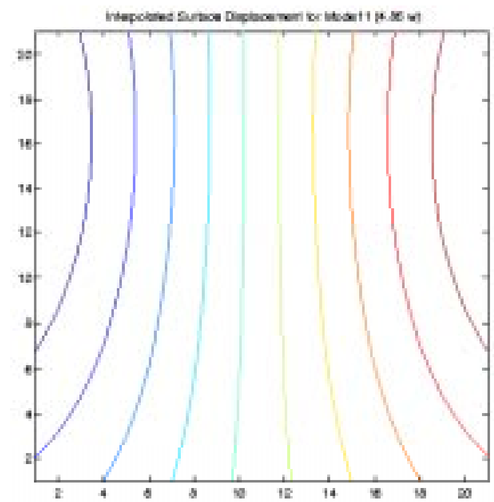

Table 5. Interpolated Mode Shapes for Z-displacement of the Front Surface Central Region (± 2.43 w)

k	*Frequency (Hz)*	*Surface Plot*	*Contour Plot*
18	12760	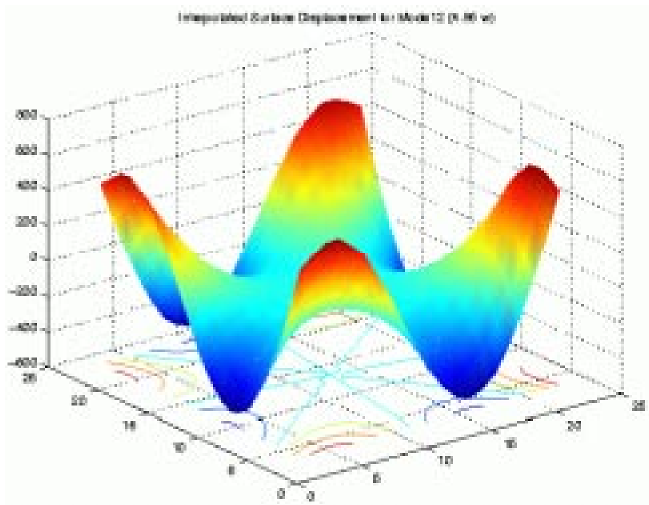	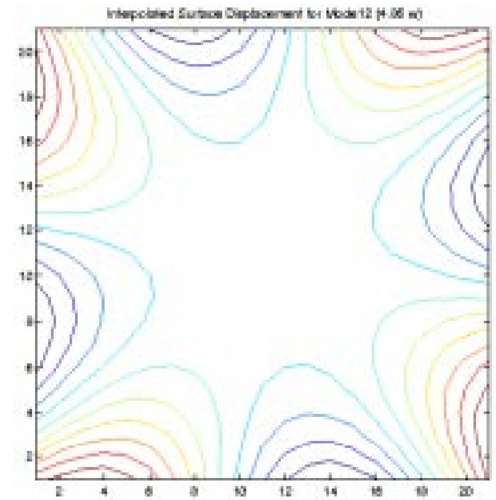
19	12760	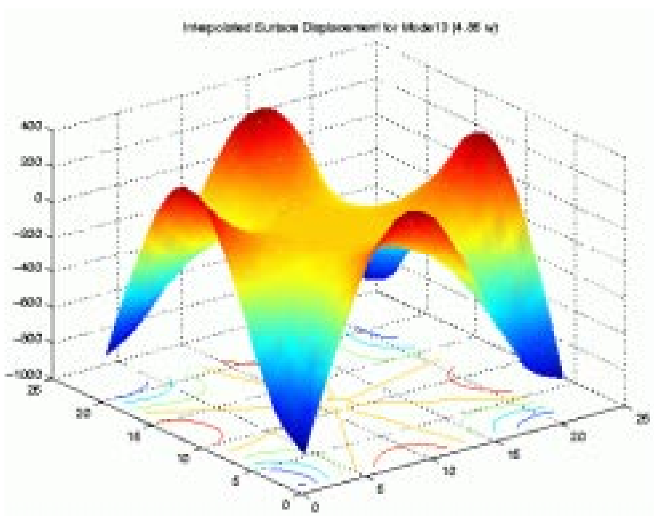	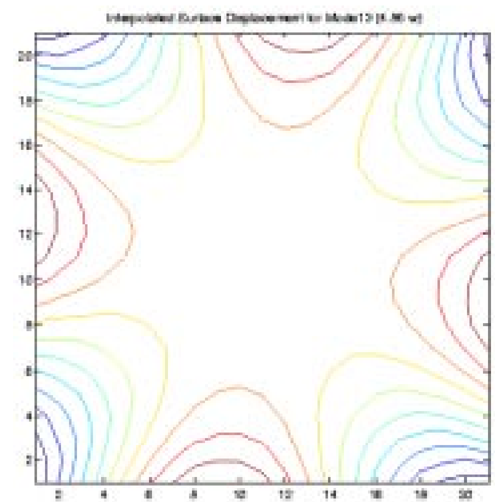

Table 5. Interpolated Mode Shapes for Z-displacement of the Front Surface Central Region (± 2.43 w)

k	*Frequency (Hz)*	*Surface Plot*	*Contour Plot*
20	14628	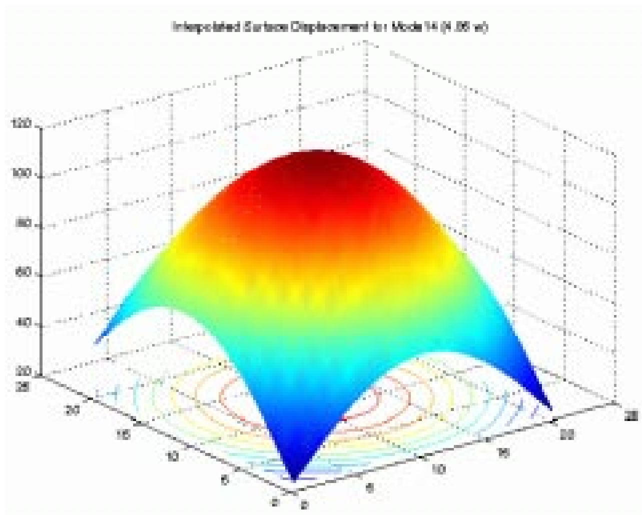	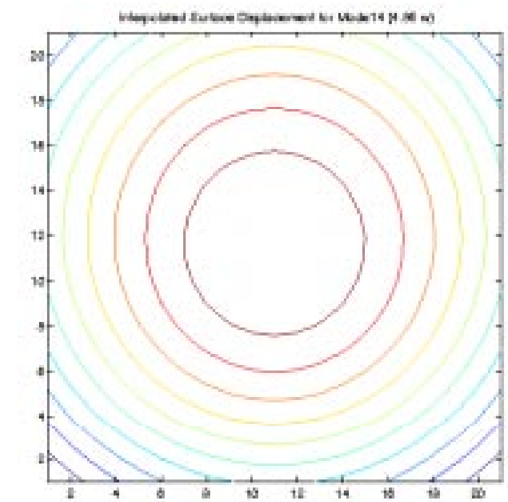

Table 5. Interpolated Mode Shapes for Z-displacement of the Front Surface Central Region (± 2.43 w)

k	*Frequency (Hz)*	*Surface Plot*	*Contour Plot*
21	17283	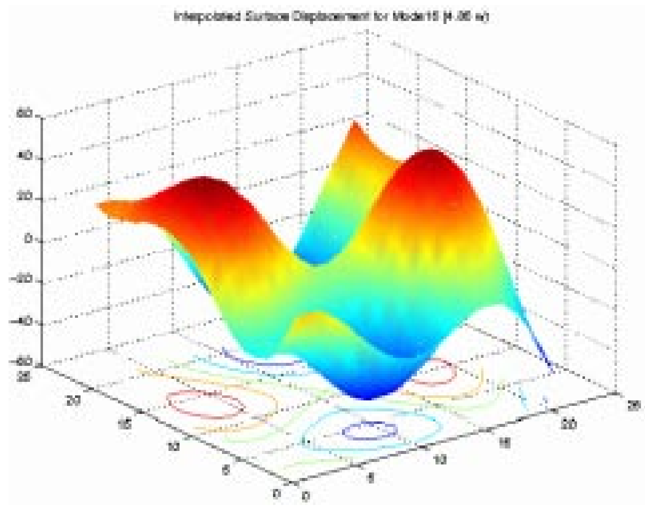	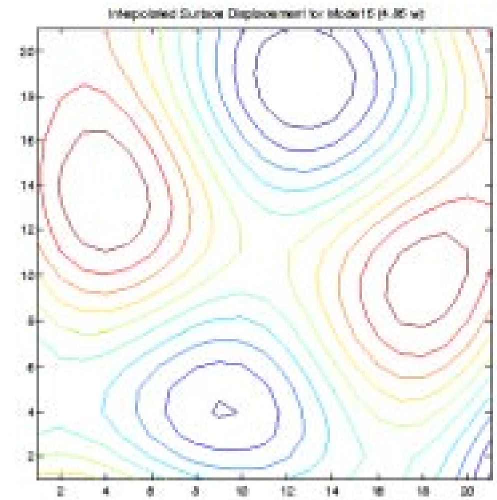
22	17283	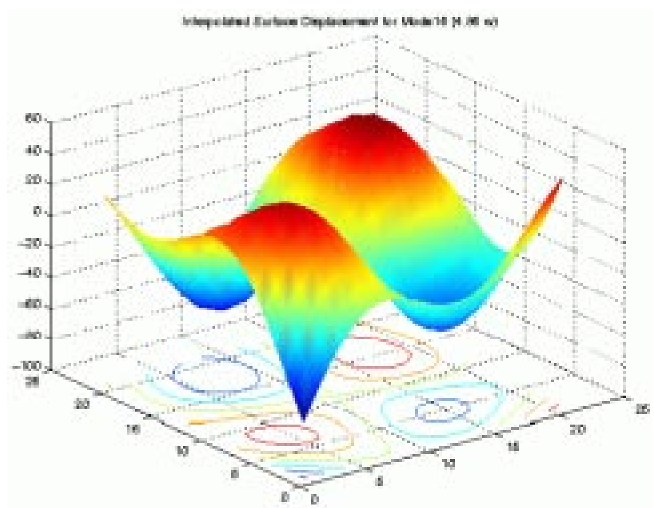	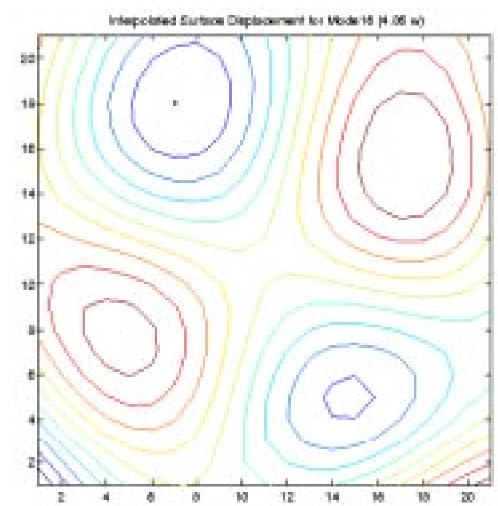

Table 5. Interpolated Mode Shapes for Z-displacement of the Front Surface Central Region (± 2.43 w)

k	*Frequency (Hz)*	*Surface Plot*	*Contour Plot*
23	17388	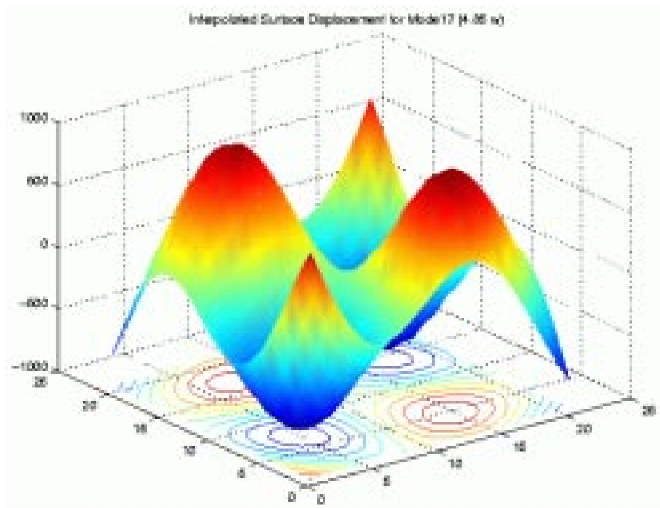	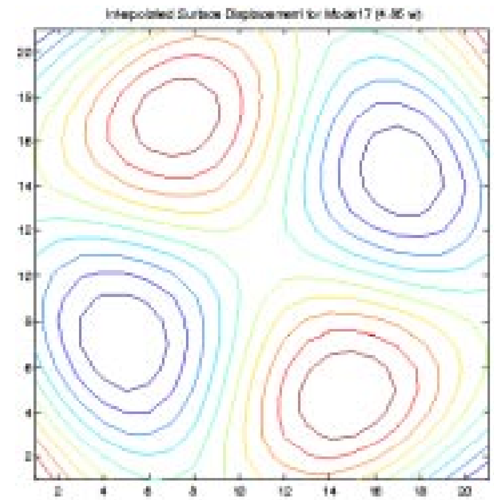

Table 5. Interpolated Mode Shapes for Z-displacement of the Front Surface Central Region (± 2.43 w)

k	*Frequency (Hz)*	*Surface Plot*	*Contour Plot*
24	17388	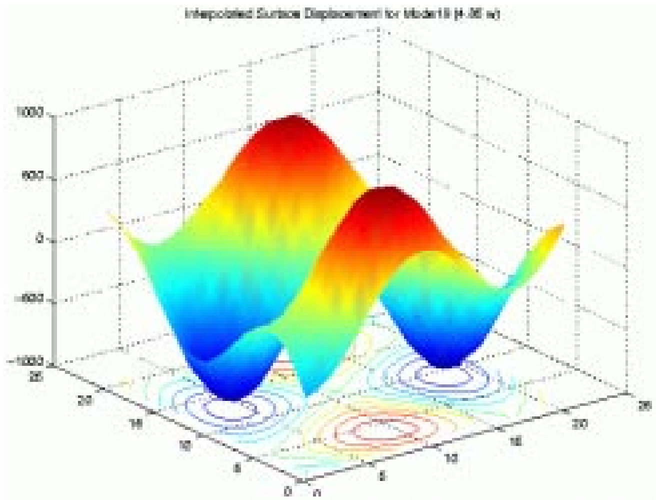	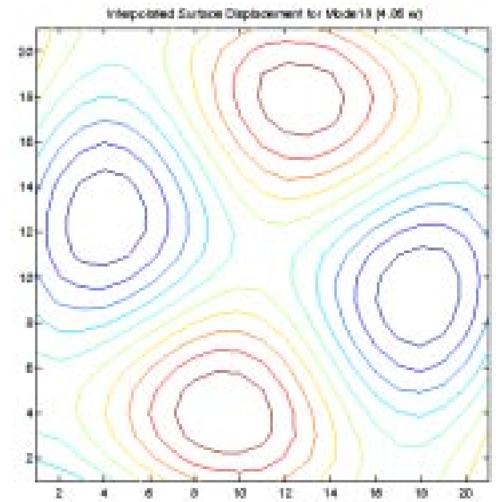

Table 5. Interpolated Mode Shapes for Z-displacement of the Front Surface Central Region (± 2.43 w)

k	*Frequency (Hz)*	*Surface Plot*	*Contour Plot*
25	17958	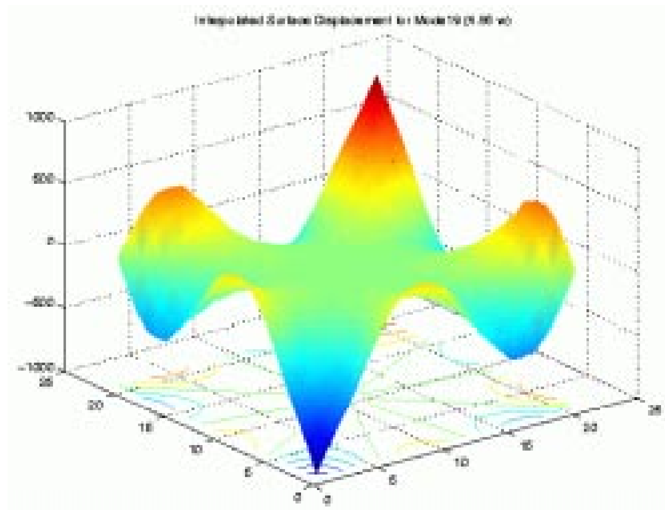	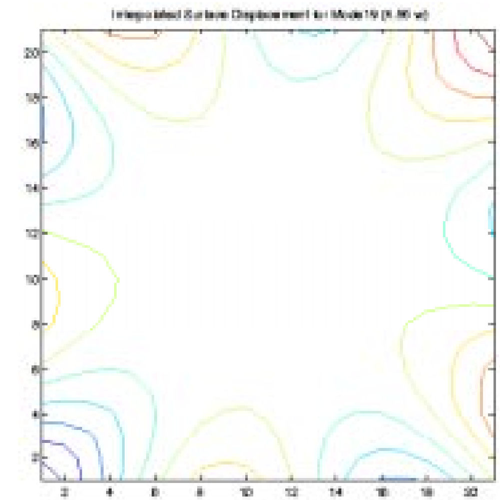
26	17958